First-Principles Investigation of the Structural, Electronic, Mechanical, and Optical Properties of A 3 NBr 3 (A = Ca, Sr, and Ba)

Conference Paper · February 2025

DOI: 10.1109/ECCE64574.2025.11014043

4 authors, including:

Bijoy Sorker
Khulna University of Engineering and Technology
5 PUBLICATIONS **7** CITATIONS

SEE PROFILE

Akash Biswas
Khulna University of Engineering and Technology
5 PUBLICATIONS **2** CITATIONS

SEE PROFILE

Abdullah Al Shadi
Khulna University of Engineering and Technology
3 PUBLICATIONS **4** CITATIONS

SEE PROFILE

2025 International Conference on Electrical, Computer and Communication Engineering (ECCE), 13-15 February 2025, CUET, Chattogram-4349, Bangladesh

First-Principles Investigation of the Structural, Electronic, Mechanical, and Optical Properties of A_3NBr_3 (A = Ca, Sr, and Ba)

Bijoy Sorker[1,*], Akash Biswas[1,†], Abdullah Al Shadi[1,‡], Sagar Mutsuddi[2,§]
[1]*Department of Electrical and Electronic Engineering, Khulna University of Engineering & Technology, Khulna, Bangladesh*
[2]*Department of Electrical and Electronic Engineering, Chittagong University of Engineering & Technology, Chittagong, Bangladesh*
sorkerbijoy.eee.kuet@gmail.com*, akash@eee.kuet.ac.bd†, abdullahalshadi7@gmail.com‡, mutsuddisagar@cuet.ac.bd§

***Abstract*—Numerous compounds from the A_3BX_3 perovskite family function as non-toxic halide perovskites, fulfilling the essential requirements for commercializing optoelectronic devices. This study thoroughly examines the structural, electronic, mechanical, and optical traits exhibited by A_3NBr_3 perovskites (where A = Ca, Sr, and Ba) through the application of density functional theory (DFT). The alternation characterized by the A site cation from Ca to Sr to Ba increases lattice constant and unit cell volume while preserving thermodynamic stability. Electronic band structure investigations unveil direct bandgaps for the investigated compounds, with a linear decrease in bandgap while changing the A site cation from Ca to Sr to Ba, rendering them beneficial for optoelectronic applications. The mechanical properties reveal that Ca_3NBr_3 and Sr_3NBr_3 are brittle, whereas Ba_3NBr_3 exhibits ductility, expanding its potential application in flexible device technologies. The change in A site cation from Ca to Sr to Ba exhibits better optical properties, encompassing favorable dielectric constants and higher absorption coefficients, making them more appropriate candidates for both photovoltaic and other optoelectronic applications. This comprehensive study elucidates the basic characteristics of A_3NBr_3 perovskites, opening up new opportunities for their integration into next-generation electronic and optoelectronic technologies.**

Keywords— DFT calculation, Lead-free perovskites, A_3BX_3, structural properties, electronic properties, direct bandgap, optical properties

I. INTRODUCTION

In today's world, propelled by fast population expansion and industrial advancement, there is an increasing energy demand. To meet demand and ensure a sustainable energy supply, it is essential to search for renewable energy resources. Solar energy remains highly regarded cost-effective and abundant long-term natural resources currently accessible. The implementation of photovoltaic (PV) technology in the energy sector is crucial since it substantially reduces fossil fuel reliance by decreasing oil consumption, mitigating emissions of greenhouse gas (GHG), and averting environmental degradation [1]. Globally, Material researchers worldwide are persistently seeking economical and novel materials to satisfy the expectations for the ongoing advancement in technology. Conventional solar cells, such as silicon, possess little potential for improvement due to their indirect and inefficient bandgaps, in addition to their prohibitively expensive manufacturing procedures [2]. Perovskite materials hold great promise for next-generation solar cell technology due to their outstanding properties. They offer high absorption coefficients, adjustable bandgaps, and excellent charge carrier mobility, leading to superior power conversion efficiencies (PCEs) compared to traditional silicon-based solar cells[3]. Inorganic perovskites are highly intriguing components for high-performance PV cells because of their outstanding opto-electronics features [4]. Inorganic perovskites are often synthesized for diverse applications in photoelectricity and energy sectors [5]Perovskite solar cells' power conversion efficiency (PCE) have shown substantial enhancement, improving from 3.8% in 2009 to a current global record of 26.1% as of 2023 [6]. The properties of perovskite materials have remarkably progressed during the last decade, facilitating its advancement [7]. The long-term stability of organic-inorganic halide perovskites (OILHP) presents significant challenges. However, the broader adoption and further advancement of lead-based perovskite solar cells are constrained by several issues, including the lead (Pb) instability within these materials, device hysteresis effects, alongside the detrimental effects of lead. These factors raise considerable concerns regarding both the environmental and human health risks associated with the production and disposal of lead-based perovskites [8].

Consequently, exploring highly efficient and economically viable inorganic halide perovskite (IHP) structures is crucial for the advancement of photovoltaic industry. Inorganic perovskites, characterized by the chemical structure A_3BX_3 (where A, B, and X are larger inorganic cation, smaller metallic cation, and anion, respectively) exhibit significant promise due to their advantageous properties such as lead-free composition, mechanical stability, superior electrical performance including high carrier mobility, and direct bandgap characteristics[9]. Ba_3SbI_3 has been recognized for its outstanding mechanical, optical, and electrical properties, rendering it appropriate for optoelectronic applications [10]. Inorganic perovskites, particularly cubic variants such as Sr_3BF_3, are promising candidates for usage in LEDs, semiconductors, and solar cells owing to their excellent optical absorption and direct bandgap

979-8-3503-5750-9/25/$31.00 ©2025 IEEE

characteristics [11]. Recent studies underscore the significance of A_3 N Cl_3 perovskites, highlighting how variations in the A-site cation critically affect their structural and electronic characteristics, thereby enhancing their suitability for usage in optoelectronic devices and solar cells [12]. Modifying the cation/halide composition at A, B, and X sites can alter the properties and enhance the performance of these materials [13]. Although A_3NBr_3 belongs to the A_3BX_3 perovskite family, it has not yet been studied. Therefore, a comprehensive investigation of these materials is necessary to address current limitations and maximize their practical applications in solar energy technologies.

In this research, we explore the structural, electronic, mechanical, and optical features of A_3 N Br_3 perovskites utilizing DFT. We aim to explore the effect of A-site cations upon the structure and band dispersion of A_3NBr_3 (A = Ca, Sr, Ba). Additionally, we examine the mechanical properties by evaluating elastic constants, various moduli, Poisson's ratio, and Pugh's ratio. We also investigate the optical characteristics of these materials to understand their photon interactions, with a focus on their potential for optoelectronic applications.

II. Computational Method

The properties of A_3NBr_3 (A = Ca, Sr, Ba) perovskites were explored utilizing first-principles density functional theory (FP-DFT) utilizing the Cambridge Serial Total Energy Package (CASTEP) [14]The exchange-correlation effect is analyzed employing the Generalized-Gradient-Approximation (GGA) in combination with the Perdew Burke Ernzerhof (PBE) functional. The Vanderbilt type ultrasoft pseudopotential was employed to evaluate the electron-ion interactions, and the Broyden Fletcher Goldfarb Shanno (BFGS) optimization method was utilized for geometric optimization. A 1000 eV plane wave cutoff energy was implemented, and an 8×8×8 k-point grid was utilized, employing the Monkhorst-Pack scheme for sampling the Brillouin zone.

The self-consistent calculations were performed using convergence thresholds that included a total energy criterion of 5.0×10^{-7} eV/atom, a maximum ionic force of 0.01 eV/Å, an ionic displacement limit of 5×10^{-4} Å, and a maximum stress limit of 0.02 GPa.

The elastic constants (C_{11}, C_{12}, and C_{44}) were computed using finite strain theory as incorporated in CASTEP. From these constants the Young's modulus (Y), the bulk modulus (B), Poisson's ratio (ν), and shear modulus (G) were calculated using Voigt-Reuss-Hill approximations. Optical calculations utilized a 16×16×16 grid of Monkhorst-Pack k-points. The real and imaginary components of the dielectric constant, absorption, reflectivity, and index of refraction are determined to assess the optical features of A_3 N Br_3 perovskites.

III. Results and Discussion

A. Structural Properties

A_3NBr_3 is a perovskite crystal exhibiting a cubic structure classified under the Pm-3m (#221) space group. Fig. 1 depicts the structural layout of A_3 N Br_3 perovskites. The A_3NBr_3 compound consists of a cubic unit cell containing a total of seven atoms, specifically 3 A atoms, 1 N atom, and 3 Br atoms. In this configuration, the A-site atoms occupy the 3d Wyckoff site with coordinates (0.5, 0, 0), while the N atom is located at the 1a Wyckoff site with coordinates (0, 0, 0). The Br atoms are located at the 3c Wyckoff site, corresponding to the coordinates (0, 0.5, 0.5). The estimated lattice constant, a (Å), and unit cell volume, V ($Å^3$), obtained using the PBE function have been presented in Table 1. Table 1 illustrates that substituting the A site cation from Ca to Sr to Ba results in an increase in both the unit cell volume and lattice constant. This phenomenon can be elucidated by the progressive enlargement of the atomic size. The formation energy, ΔE_f of A_3 N Br_3 perovskites are computed by the following expression and enlisted in Table 1 to justify their phase stability.

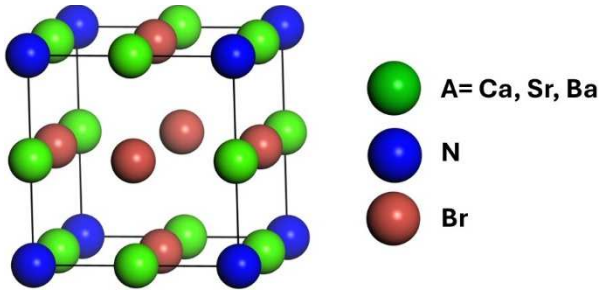

Fig. 1. The crystal arrangement of A_3NBr_3 perovskites after optimization.

TABLE I. ESTIMATED LATTICE CONSTANT (A), UNIT CELL VOLUME (V), AND FORMATION ENERGY (ΔE_f) OF A_3NBr_3 PEROVSKITES

Compound	*a* (Å)	*V* ($Å^3$)	ΔE_f *(eV/atom)*
Ca_3NBr_3	5.64	179.70	-4.19
Sr_3NBr_3	5.97	213.81	-4.15
Ba_3NBr_3	6.35	256.90	-4.06

$$\Delta E_f(A_3NBr_3) = \frac{[E_{tot.}(A_3NBr_3) - 3E(A) - E(N) - 3E(Br)]}{n} \quad (1)$$

Here, in equation (1), E(A), E(N), and E(Br) represent the energies of the individual atoms A (Ca, Sr, Ba), N, and Br atoms, respectively, while, $E_{tot.}(A_3NBr_3)$ denotes the unit cell's total energy of A_3NBr_3. Here, n corresponds to the atoms' number within the unit cell. The negative quantities of ΔE_f for the studied structures indicate their stable thermodynamic configuration.

B. Electronic Properties

Investigating the band structure is crucial for assessing the electronic characteristics of a compound. The band structures of A_3 N Br_3 perovskites have been calculated with the Brillouin zone path X-R-M- Γ-R employing GGA-PBE functional are depicted in Fig. 2. Consistent with semiconductor theory, the electronic band structure close to Fermi level (E_F) plays a pivotal role in understanding the material's physical properties. Therefore, we have presented the band structures within the energy range surrounding the Fermi level (-6 to 6 eV), with (E_F) positioned at 0 eV. Fig. 2 (a-c) illustrates that the valence band maximum (VBM) and conduction band minimum (CBM) are positioned at the Γ point within the Brillouin zone, confirming the direct band gap nature of all the investigated compounds. Direct band gap

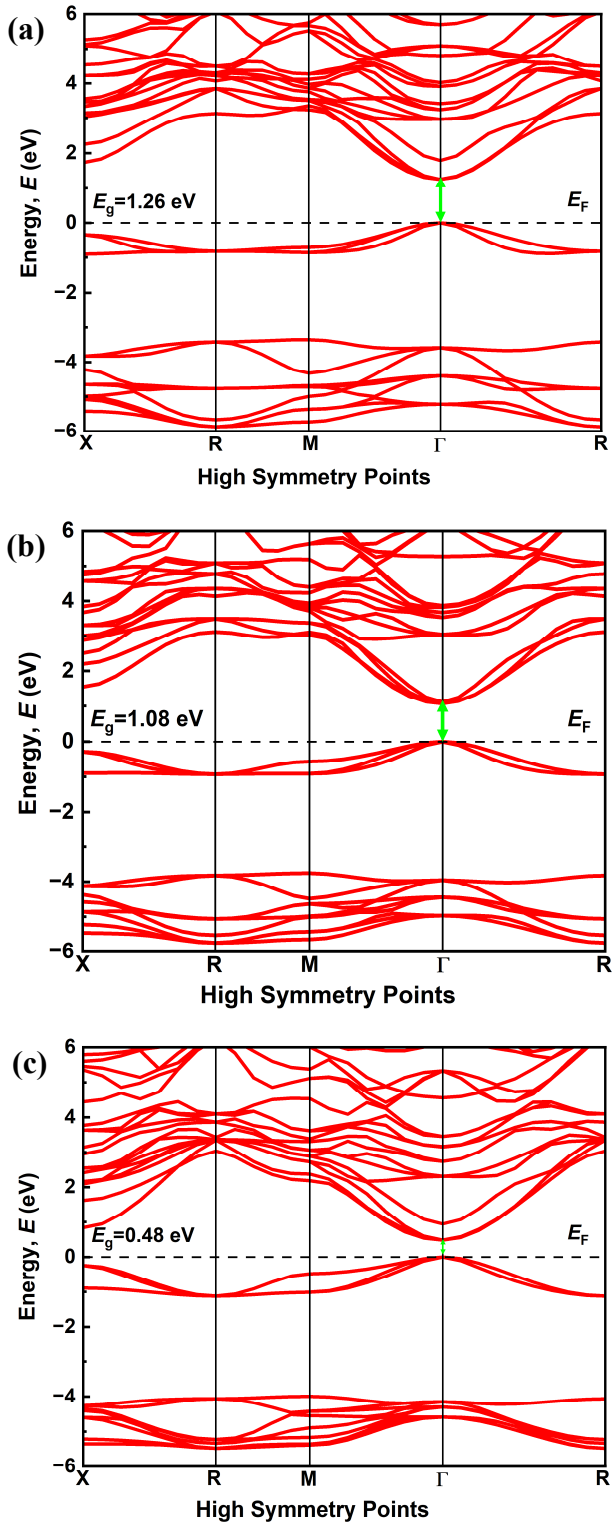

Fig. 2. Computed energy band configurations of (a) Ca_3NBr_3, (b) Sr_3NBr_3, and (c) Ba_3NBr_3 perovskites using GGA method.

semiconductors are in high demand for their potential use in optoelectronic, photovoltaic, and photothermal applications [12]. The direct band gaps for Ca_3NBr_3, Sr_3NBr_3, and Ba_3NBr_3 are found to be 1.26 eV, 1.08 eV, and 0.48 eV respectively. The energy band gap values for the examined compounds exhibit a gradual decrease as the cation occupying the A-site transitions from Ca, Sr, and Ba in succession. The ionic radii of Ca, Sr, and Ba cations influence the arrangement of adjacent Br atoms and affect the interatomic spacing.

As the A site cation radius rises, the spacing between adjacent atoms also increases weakening of the electrostatic interactions between the cations and Br atom. This results in the band gap's (E_g) reduction facilitating more efficient and rapid electron transitions from the lower energy band to the higher energy band.

C. Mechanical Properties

Solid materials' mechanical properties encompass different attributes including strength, elasticity, wear resistance, flexibility or brittleness, hardness, machinability, and toughness. This study presents the elastic constants of A_3NBr_3, which, due to its cubic symmetry, possesses three independent elastic constants (C_{ij}). For ensuring mechanical stability according to the Born–Huang criteria, [20] the system must satisfy the following inequality conditions: $C_{11} > 0$, $C_{44} > 0$, C_{11}-$C_{12} > 0$, and $C_{11} + 2C_{12} > 0$.

Several mechanical properties of A_3NBr_3 perovskites, including the bulk modulus (B), shear modulus (G), Young's modulus (Y), Poisson's ratio (ν) and Pugh's ratio (B/G) were computed from the elastic constants. Consequently, B and G were calculated utilizing the Voigt-Reuss formalism, which establishes the range for the effective moduli of cubic lattices.

Hill's theory asserts that B and G are the arithmetic averages of the Voigt and Reuss limits. Moreover, E and ν are subsequently determined by using standard equations. And B

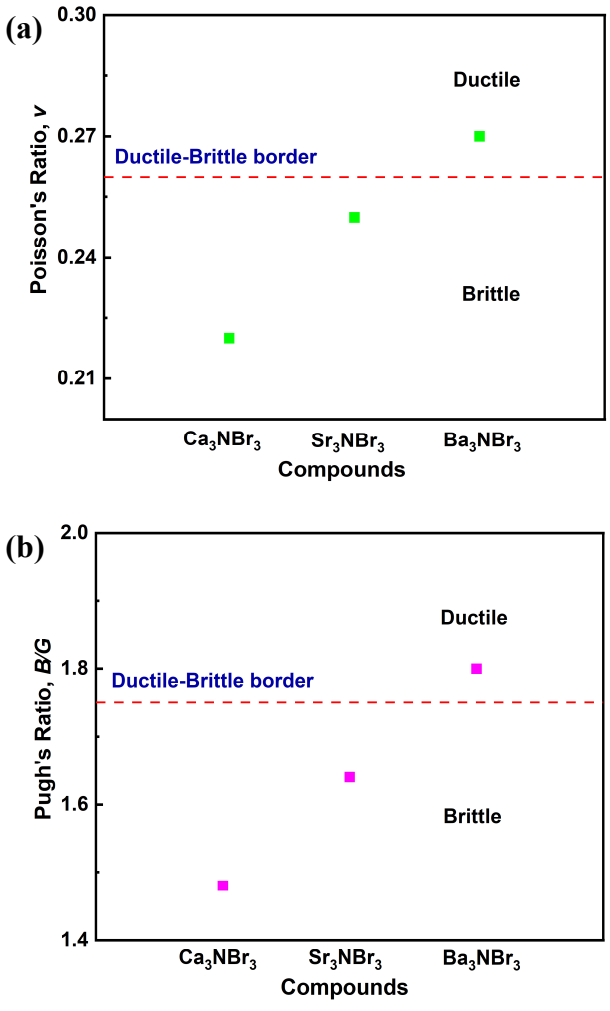

Fig. 3. Variation of (a) Poisson's ratio, and (b) Pugh's ratio with A-site cation in cubic inorganic A_3NBr_3 perovskites.

serves as an exhibitor of a material's resistance to fracture, whereas G signifies its ability to withstand plastic deformation.

Elevated values B and G imply that Ca_3NBr_3 exhibits greater resistance to both fracture and plastic deformation in comparison to Ba_3NBr_3 and Sr_3NBr_3. Additionally, Young's modulus confirms that Ca_3NBr_3 exhibits greater stiffness than the other two compounds. As A site cation radius increases from Ca to Ba, properties such as fracture resistance, resistance to plastic deformation, and stiffness progressively decline.

Ductility is an important property of solid materials that affects their ability to be shaped and processed in industrial applications. In optoelectronics, ductile materials are essential for creating flexible devices, which have great potential in bioelectronics and emerging energy technologies. Both the B/G ratio (bulk-to-shear modulus ratio) and ν (Poisson's ratio) are used to assess a material's ductility. Materials are considered brittle if the B/G ratio is less than 1.75 and Poisson's ratio is less than 0.26. On the other hand, materials are classified as ductile if the B/G ratio is greater than 1.75 and Poisson's ratio is greater than 0.26[16]. Our investigations indicate that Ba_3NBr_3 is ductile, while Ca_3NBr_3 and Sr_3NBr_3 are brittle, broadening the application scope for stable Ba_3NBr_3. From Fig. 3 it is noticed that as the A site cation transitions from Ca to Sr to Ba, brittleness decreases and ductility increases.

D. Optical Properties

The frequency-dependent optical characteristics of a molecule reveal its interaction with electromagnetic radiation, which in turn affects several applications in telecommunications, medicine, optoelectronics, and photovoltaics. Quantum mechanics, utilizing DFT, provides a structured framework for investigating the optical properties of electrons in materials. Electrons undergo energy state transitions when interactions occur between photons of a certain energy and matter. This study involved the analysis of several parameters, encompassing the complex dielectric-function ε(ω), reflectivity R(ω), index of refraction n(ω), and coefficient of absorption α(ω).

The complex dielectric function, $\varepsilon(\omega)= \varepsilon_1(\omega)+i\,\varepsilon_2(\omega)$, comprises both real and imaginary components, represented by $\varepsilon_1(\omega)$ and $\varepsilon_2(\omega)$, respectively. The real part, $\varepsilon_1(\omega)$, indicates the material's response to light transmission, whereas the imaginary part, $\varepsilon_2(\omega)$, corresponds to the degree of light absorption within the compound. Fig. 4(a) presents the dielectric function's real component in relation to photon energy, spanning the energy range of 0 to 40 eV. At zero energy the static dielectric constant is represented by $\varepsilon_1(0)$ takes the values of 5.9, 5.9, and 7.5 for Ca_3NBr_3, Sr_3NBr_3, and Ba_3NBr_3 respectively.

TABLE II. CALCULATED MECHANICAL PROPERTIES OF A_3NBr_3 PEROVSKITES.

Parameters	Symbol	Compounds		
		Ca_3NBr_3	Sr_3NBr_3	Ba_3NBr_3
Elastic Constants	C_{11}	94.95	84.08	70.71
	C_{12}	16.07	14.07	11.29
	C_{44}	22.92	17.07	11.77
Bulk Modulus	B (GPa)	42.36	37.41	31.09
Shear Modulus	G (GPa)	28.53	22.86	17.24
Young Modulus	Y (GPa)	69.90	56.97	43.65
Poisson's Ratio	*c*	0.22	0.25	0.27
Pugh's Ratio	B/G	1.48	1.64	1.8

The highest peaks observed for Ba_3NBr_3, Sr_3NBr_3, and Ca_3NBr_3, are 0.5 eV, 1.25 eV, and 1.5 eV respectively. The estimated values for the static dielectric constant $\varepsilon_1(0)$ and the bandgap value aligns with Penn's model [17] A negative dielectric function (ε_1) was observed in the energy range of ~ 8.5eV and ~27.5eV, indicating no wave propagation within this energy range.

The dielectric function's imaginary part is inherently connected to the material's band structure and provides insight into its absorption characteristics. Fig. 4(b) depicts the estimated ε_2 (ω) values plotted against photon energy, demonstrating energy dissipation and electronic transitions across the bandgap. This graph illustrates significant absorption within energy ranging from 0.85 to 29.5 eV, proposing that these compounds possess strong potential for application in photovoltaic technologies. Furthermore, the absorption observed within the range of 20–25 eV suggests promising applications within the ultraviolet (UV) spectrum-based technologies, such as medical therapies [18]. Fig. 4(b) demonstrates that the dielectric function's imaginary component, ε_2 (ω), for Ba_3NBr_3 exhibits superior performance compared to Sr_3NBr_3 and Ca_3NBr_3, particularly in the energy spectrum of photons from 15 eV to 30 eV, where its peaks are significantly higher. This enhanced absorption in Ba_3NBr_3 can be attributed to its larger atomic mass and higher electron density, resulting in stronger photon-electron interactions. The presence of Ba, a heavier alkaline earth metal compared to Sr and Ca, leads to increased polarization and electron excitation at higher energy levels. Consequently, Ba_3NBr_3 demonstrates a broader absorption spectrum and stronger photon absorption in the extreme ultraviolet (EUV) range, making it more suitable for high-energy applications, such as EUV lithography, where efficient energy absorption is critical. In contrast, Sr_3NBr_3 and Ca_3NBr_3 exhibit lower absorption peaks, indicating their optimal performance in lower-energy ultraviolet (UV) applications. Thus, the electronic structure and material composition of Ba_3NBr_3 plays a pivotal role in its superior optical properties in the high-energy spectrum.

The frequency-dependent refractive index $n(\omega)$ characterizes how electromagnetic radiation interacts with a medium. It can be observed from Fig. 5(a), the refractive indices of Ba_3NBr_3, Sr_3NBr_3, Ca_3NBr_3 exhibit distinct trends across the photon energy spectrum. In the lower energy range (below 5 eV), all materials show high refractive indices, demonstrating robust interactions between light and matter within the ultraviolet (UV) spectrum. As photon energy increases, the refractive index decreases, with Ba_3NBr_3 displaying pronounced fluctuations between 10 and 30 eV, suggesting more complex electronic transitions. This highlights that Ba_3NBr_3 shows greater sensitivity to high-energy photons compared to Sr_3NBr_3 and Ca_3NBr_3. At energies above 30 eV, the refractive indices converge, indicating diminished interaction in the extreme ultraviolet (EUV) region. These variations emphasize Ba_3NBr_3 has more potentiality for high-energy optical applications, while smoother behavior of Ca_3NBr_3 suggests it's stability for lower-energy environments.

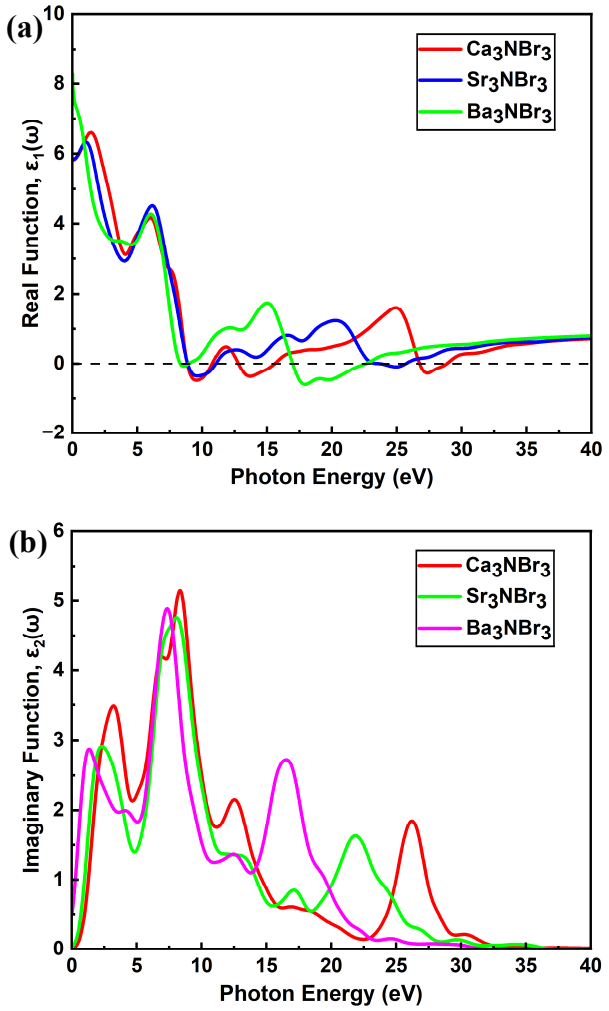

Fig. 4. Calculated (a) real and (b) imaginary dielectric functions of A_3NBr_3 perovskites.

The coefficient of absorption indicates the amount of light absorbed per unit thickness before the intensity becomes negligible. This property is crucial for optimizing a material's performance in high-efficient solar cells and other photovoltaic applications. Fig. 5(b) illustrates the absorption spectra of A_3NBr_3 structures in relation to photon energy. The absence of absorption at specific photon energy levels corroborates the semiconducting properties of these materials, with absorption commencing at approximately 1.5 eV. As photon energy increases, absorption rises, peaking in the UV range for all structures, rendering them appropriate for ultraviolet-sensitive optoelectronic applications, including radiation detectors and scintillators. Reflectivity R(ω) indicates how efficiently the material reflects incoming light rather than absorbing or transmitting it. The total reflectance of perovskite materials can exhibit substantial variations over surface morphology, crystal orientations, and composition. Furthermore, the reflectivity of A_3NBr_3 perovskite might be influenced due to the wavelength and incident light angle. Shown in Fig. 5(c) are the reflectivity profiles for the substances being studied. At 0.175eV for Ca_3NBr_3, 0.175eV for Sr_3NBr_3, and 0.215eV for Ba_3NBr_3, the figure depicts threshold reflectivity values. Spectral reflection responses of all substances vary above zero frequency. This study reveals that Ca_3NBr_3, Sr_3NBr_3 and Ba_3NBr_3 exhibit significant reflection, with highest values of 30% at 9 eV, 28% at 9 eV, and 37% at 21 eV, respectively.

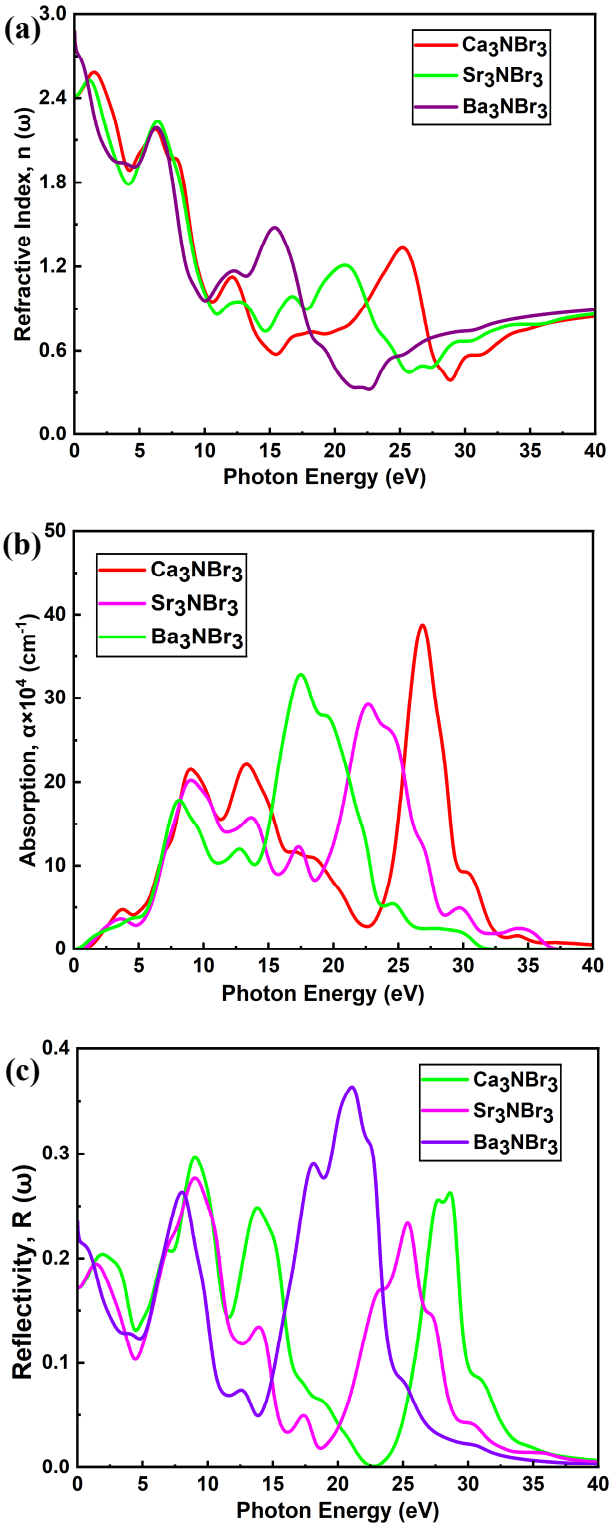

Fig. 5. Computed optical spectra of (a) refractive index, (b) absorption coefficient, and (c) reflectivity of A_3NBr_3 perovskites.

Ca_3NBr_3 and $Sr_3NBr_3$are best suited for UV applications since their reflection peaks occur at 9 eV, within the UV range. These materials would be efficient at reflecting ultraviolet light, making them useful for UV filters, mirrors, or coatings. Ba_3NBr_3 is best for high-energy EUV applications, as its reflection peak occurs at 21 eV, within the EUV spectrum. This makes it optimal for applications requiring the reflection of high-energy light, such as EUV lithography, used in semiconductor manufacturing.

IV. Conclusion

To conclude, the structural, mechanical, electronic, and optical properties of lead-free inorganic A_3NBr_3 perovskites were examined utilizing the DFT-based CASTEP module. The A_3 N Br_3 compounds exhibit both structural and thermodynamic stability. The bandgap values calculated with the GGA-PBE method are 1.26eV for Ca_3NBr_3, 1.08eV for Sr_3NBr_3, and 0.48eV for Ba_3NBr_3. A clear pattern emerges: as the diameter of the cation increases (Ba > Sr > Ca), the bandgap decreases. This trend suggests that these materials could be useful for different optoelectronic applications. Furthermore, all investigated perovskites are mechanically stable, as indicated by their elastic constants. Specifically, Ca_3NBr_3 and Sr_3NBr_3 exhibit brittle characteristics, while Ba_3NBr_3 is ductile. The optical properties analysis further suggests that $Ba_3NBr_3$is the best candidate for photovoltaic cell compared to Ca_3NBr_3 and Sr_3NBr_3. Because it shows superior dielectric constant, and strong reflectivity. The valuable outcomes from our simulations are expected to help in the experimental design of high performing optoelectronic devices based on A_3NBr_3.

References

[1] M. K. Hossain *et al.*, "Harnessing the potential of $CsPbBr_3$ -based perovskite solar cells using efficient charge transport materials and global optimization," *RSC Adv*, vol. 13, no. 30, pp. 21044–21062, Jul. 2023.

[2] M. F. Rahman *et al.*, "Concurrent investigation of antimony chalcogenide (Sb_2Se_3 and Sb_2S_3)-based solar cells with a potential WS2 electron transport layer," *Heliyon*, 2022.

[3] N. Rahman *et al.*, "First Principle Study of Structural, Electronic, Elastic, and Magnetic Properties of Half-Heusler Compounds ScTiX (X = Si, Ge, Pb, In, Sb, and Tl)," *J Supercond Nov Magn*, 2020.

[4] M. K. Hossain *et al.*, "Deep Insights into the Coupled Optoelectronic and Photovoltaic Analysis of Lead-Free $CsSnI_3$ Perovskite-Based Solar Cell Using DFT Calculations and SCAPS-1D Simulations," *ACS Omega*, vol. 8, no. 25, pp. 22466–22485, Jun. 2023.

[5] M. A. Green, A. Ho-Baillie, and H. J. Snaith, "The emergence of perovskite solar cells," 2014.

[6] P. Cheng, Y. An, A. K. Y. Jen, and D. Lei, "New Nano photonics Approaches for Enhancing the Efficiency and Stability of Perovskite Solar Cells," *Advanced Materials*, vol. 36, no. 17, p. 2309459, Apr. 2024.

[7] H. S. Jung and N. G. Park, "Perovskite solar cells: From materials to devices," 2015.

[8] Q. Wang and A. Abate, "Perovskite Solar Cells: Promises and Challenges," in *Emerging Photovoltaic Materials*, 2018.

[9] A. Ghosh *et al.*, "Investigating of novel inorganic cubic perovskites of A_3BX_3 (A=Ca, Sr, B[dbnd]P, As, X=I, Br) and their photovoltaic performance with efficiency over 28%," *J Alloys Compd*, 2024.

[10] M. F. Rahman *et al.*, "A computational study of electronic, optical, and mechanical properties of novel Ba_3SbI_3 perovskite using DFT," *Opt Quantum Electron*, vol. 56, no. 2, pp. 1–23, Feb. 2024.

[11] M. Hasan *et al.*, "A comprehensive analysis of structural, electronic, optical, mechanical, thermodynamic, and thermoelectric properties of direct band gap Sr_3BF_3 (B = As, Sb) photovoltaic compounds: DFT-GGA and mBJ approach," *Inorg Chem Commun*, vol. 171, p. 113607, Jan. 2025.

[12] M. A. Rahman *et al.*, "Impact of A-Cations Modified on the Structural, Electronic, Optical, Mechanical, and Solar Cell Performance of Inorganic Novel A_3NCl_3 (A = Ba, Sr, and Ca) Perovskites," *Energy and Fuels*, vol. 38, no. 9, pp. 8199–8217, May 2024.

[13] H. Zhu *et al.*, "Organic Cations Might Not Be Essential to the Remarkable Properties of Band Edge Carriers in Lead Halide Perovskites," *Advanced Materials*, 2017.

[14] "Materials Studio 2023 - CASTEP." Accessed: Oct. 05, 2024. [Online].

[15] M. Born, "On the stability of crystal lattices. I," *Mathematical Proceedings of the Cambridge Philosophical Society*, vol. 36, no. 2, pp. 160–172, 1940.

[16] S. F. Pugh, "XCII. Relations between the elastic moduli and the plastic properties of polycrystalline pure metals," *The London, Edinburgh, and Dublin Philosophical Magazine and Journal of Science*, 1954.

[17] D. R. Penn, "Wave-number-dependent dielectric function of semiconductors," *Physical Review*, 1962.

[18] J. Itoh and Y. Itoh, "A New Drug-Free Cancer Therapy Using Ultraviolet Pulsed Irradiation. PDT (Photo Dynamic Therapy) to PPT (Pulsed Photon Therapy)," *Frontiers in Bioscience - Scholar*, 2022.